THE JOURNAL OF PHYSICAL CHEMISTRY LETTERS
A JOURNAL OF THE AMERICAN CHEMICAL SOCIETY

pubs.acs.org/JPCL

Letter

Visualizing Stereodynamics in Cold Collisions through Shape Resonance Wavefunctions

Yilang Liu,* Dongzheng Yang, Hua Guo, and Daiqian Xie*

Cite This: *J. Phys. Chem. Lett.* 2025, 16, 1796−1801

Read Online

ACCESS | Metrics & More | Article Recommendations | Supporting Information

ABSTRACT: Shape resonances in cold collisions are often strongly affected by stereodynamics. These resonances can sometimes be assigned by single-channel quantization along the scattering coordinate. However, sensitive steric control of collision implies strong anisotropy of the interaction potential energy surface, which usually leads to coupling among multiple scattering channels in the strongly interacting region. Hence, the resonances might be the result of quantization in a multidimensional space. Using the cold rotationally inelastic collision between *para*-H_2 ($v_1 = 1$, $j_1 = 2$) and HF ($v_2 = 0$, $j_2 = 0$) as an example, we analyze four low-lying shape resonances via diagonalization of the full-dimensional Hamiltonian with a stabilization method. While some resonances can indeed be assigned with a single partial wave, others apparently involve more than one scattering channel. A new model based on these resonance wavefunctions is developed to better understand the stereodynamics through shape resonances in cold collisions.

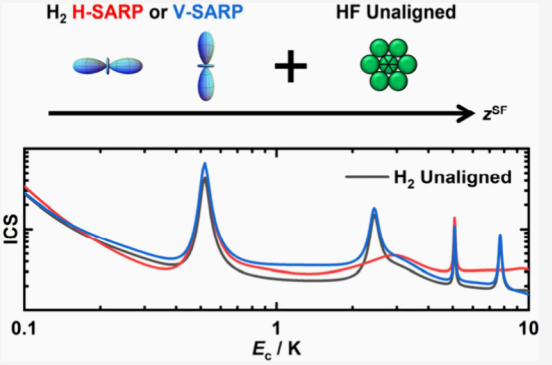

Complete control of molecular scattering at the quantum state level is a long sought-after goal in chemical physics. The ultimate challenge to attain such control is to understand the correlation between oriented or aligned collision partners and the scattering outcomes. Fundamentally, this so-called stereodynamics stems from the anisotropy of the interaction potential energy surface (PES),[1] but not always in a predictable way. In recent years, experimental preparations of oriented or aligned molecules have advanced to an unprecedented level that allowed the study of stereodynamics of both reactive and nonreactive collisions.[2−10]

In the cold regime with collision energies on the order of 1 K, scattering is typically dominated by one or a few partial waves. As a result, quantum effects such as resonances become prominent.[11,12] In recent work by Zare and co-workers, for example, shape resonances have been detected in cold collisions between HD and D_2,[13] as well as other isotopomers,[14−16] and shown to be strongly affected by initial orientation of one or both collision partners. The initial preparation of molecules in a direction parallel or perpendicular to the relative velocity of the collision partners was made possible by Stark-induced adiabatic Raman passage (SARP) and the cold collision temperature was achieved in a copropagating beam.[8] Quantum mechanical studies of these processes have revealed the nature of the shape resonances dominated by single partial waves,[17−19] which helped to gain fundamental insights of stereodynamical control of collision dynamics via resonances.[20]

Different from a Feshbach resonance in which an internal mode is excited, a shape resonance is a metastable state formed by the shape of the interaction PES. For nonreactive scattering, shape resonances can form in the potential well resulted from van der Waals or hydrogen bond interactions between the colliding molecules. For the $H_2 + H_2$ system,[17] for example, the anisotropy of the PES is relatively weak. As a result, the shape resonances are largely localized in large intermolecular distances and can often be assigned by examining the one-dimensional (1D) quantum states in the scattering coordinate (R) in the relevant scattering channel labeled by the incoming orbital angular momentum (L). They correspond to quasi-bound states supported by the effective potential ($V(R)+L(L+1)\hbar^2/2\mu R^2$)) where $V(R)$ is the channel-averaged interaction potential and μ is the collisional reduced mass. For strongly interacting systems, this single-channel model may no longer be appropriate, due to the coupling of the scattering coordinate with other molecular modes dictated by the anisotropic PES. Indeed, in a recent study of the cold H_2 + HCl collision, two low-lying resonance peaks could not be assigned within the 1D model.[21] Such difficulties hinder our understanding of the stereodynamics. In other systems, it might even be difficult to distinguish between the shape and Feshbach resonances.

Received: December 27, 2024
Revised: February 1, 2025
Accepted: February 6, 2025

https://doi.org/10.1021/acs.jpclett.4c03703
J. Phys. Chem. Lett. 2025, 16, 1796−1801

In this Letter, we investigate rotationally inelastic scattering in another strongly anisotropic system,[22,23] *para*-H_2 ($v_1 = 1$, $j_1 = 2$) + HF ($v_2 = 0$, $j_2 = 0$) → *para*-H_2 ($v'_1 = 1$, $j_1' = 0$) + HF ($v_2' = 0$, j_2'), in the cold regime. Full-dimensional quantum scattering calculations are carried out and stereodynamics analyzed. Similar to the H_2 + HCl system,[21] some of the low-lying resonances are difficult, if not impossible, to assign within the 1D model. To better understand these resonances and their impact on stereodynamics, we calculate the resonance wavefunctions by diagonalizing full-dimensional Hamiltonian using a stabilization method. Furthermore, we device a model to identify the role played by these resonances in controlling the stereodynamics.

Full-dimensional time-independent close-coupling (TICC) calculations on a highly accurate H_2−HF PES,[23,24] which is augmented by a long-range interaction term (see Section S−II of Supporting Information (SI) for detail), were performed employing a homemade 2 + 2 code.[25] In the helicity representation,[26] the following scattering amplitudes

$$
\begin{aligned}
&q_{\alpha',m_1',m_2',m_{12}'\leftarrow\alpha,m_1,m_2,m_{12}}(\theta; E_c)\\
&= \frac{1}{2k_\alpha}\sum_J (2J+1)\sum_{j'_{12}L'j_{12}L} i^{L-L'+1}T^J_{\alpha'j'_{12}L',\alpha j_{12}L}(E_c)d^J_{m_{12},m'_{12}}(\theta)\\
&\times \langle j'_{12}m'_{12}J(-m'_{12})|L'0\rangle\langle j_{12}m_{12}J(-m_{12})|L0\rangle\\
&\times \langle j'_1m'_1j'_2m'_2|j'_{12}m'_{12}\rangle\langle j_1m_1j_2m_2|j_{12}m_{12}\rangle
\end{aligned}
\tag{1}
$$

are needed to calculate the differential and integral cross sections (DCSs and ICSs). Here, a combined molecular state (CMS) is labeled by $\alpha = (v_1j_1v_2j_2)$, where the subscript 1 is for H_2 and 2 is for HF. E_c is the collision energy, $k_\alpha = \sqrt{2\mu E_c}$, $\mu = \frac{m_{H_2}m_{HF}}{m_{H_2}+m_{HF}}$, J, L are the total and orbital angular momenta, and $\mathbf{j}_{12} = \mathbf{j}_1 + \mathbf{j}_2$ with m_{12}, m_1, m_2 as the corresponding z-components in the space-fixed (SF) coordinate frame illustrated in Figure S1. The transmission matrix is related to the scattering matrix: $T^J = 1 - S^J$, and $d^J_{m_{12},m'_{12}}(\theta)$ is the Wigner reduced rotation matrix element.

In a SARP experiment in which the H_2 molecule is prepared in a fixed initial internal state with its principal axis at an angle β relative to the H_2−HF relative velocity as

$$
|j_1\rangle^{\text{aligned},\beta} = \sum_{m_1} d^{j_1}_{0,m_1}(\beta)|j_1m_1\rangle \tag{2}
$$

the DCS is given as

$$
\frac{d\sigma^{\text{aligned},\beta}_{\alpha'\leftarrow\alpha}(\theta; E_c)}{d\Omega} = \frac{1}{(2j_2+1)}\times \sum_{m'_1m'_2m'_{12}m_2m_{12}}\left|\sum_{m_1} d^{j_1}_{0,m_1}(\beta)q_{\alpha',m'_1,m'_2,m'_{12}\leftarrow\alpha,m_1,m_2,m_{12}}(\theta; E_c)\right|^2 \tag{3}
$$

to account for the interference between different polarized states in the entrance channel preparation,[17] and the ICS can be calculated by the integral

$$
\sigma^{\text{aligned},\beta}_{\alpha'\leftarrow\alpha}(E_c) = 2\pi\int_0^\pi \sin\theta d\theta \frac{d\sigma^{\text{aligned},\beta}_{\alpha'\leftarrow\alpha}(\theta; E_c)}{d\Omega} \tag{4}
$$

For randomly oriented/aligned collisional partners, averaging over m_1 yields the corresponding cross sections.

The calculated ICS for nonpolarized rotationally inelastic collisions, *para*-H_2 ($v_1 = 1$, $j_1 = 2$) + HF ($v_2 = 0$, $j_2 = 0$) → *para*-H_2 ($v_1' = 1$, $j_1' = 0$) + HF ($v_2' = 0$, $j_2' = 3$), as a function of E_c is shown in Figure 1(a), featuring four prominent

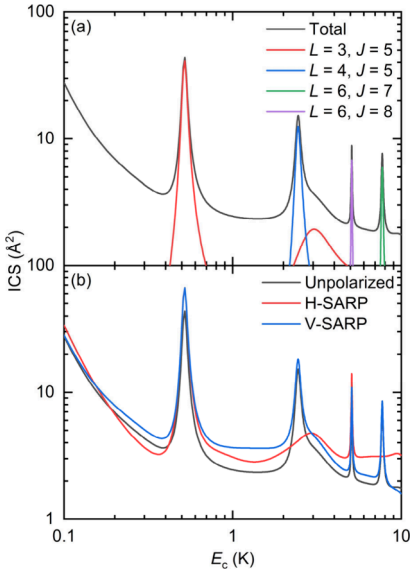

Figure 1. Integral cross sections for *para*-H_2 ($v_1 = 1$, $j_1 = 2$) + HF ($v_2 = 0$, $j_2 = 0$) → *para*-H_2 ($v_1' = 1$, $j_1' = 0$) + HF ($v_2' = 0$, $j_2' = 3$). (a) Partial wave resolved ICSs. (b) ICSs for different initially aligned H_2.

resonance peaks at 0.52 (Peak 1), 2.44 (Peak 2), 5.08 (Peak 3), and 7.71 K (Peak 4), dominated by the (L, J) = (3, 5), (4, 5), (6, 8) and (6, 7) contributions, respectively. Figure 1(b) shows the sensitivity of these resonances to the initial H_2 alignment specified by the β angle: Peaks 2 and 4 are largely switched off in H-SARP ($\beta = 0$), whereas no qualitative difference between the V-SARP ($\beta = 90°$) and isotropic ICS was observed. Note that the (L, J) = (3, 5) partial wave also leads to a broader scattering resonance around 3 K, but it is obscured by Peak 2 when H_2 is unaligned or aligned by V-SARP. However, it becomes prominent in H-SARP due to the disappearance of Peak 2. ICSs in the other three energetically accessible exit channels, $j_2' = 0$, 1 and 2, do not show significant differences except for two resonance peaks due to the conservation of J and parity ε (±1 refers to even/odd parity), as illustrated in Section S−III of SI.

In order to gain further insight into the quantum nature of these resonances and corresponding stereodynamical preferences, we first attempted to assign them based on the widely used 1D model with the following effective potential:

$$
V^{\text{eff}}_{\alpha j_{12}LJ}(R) = \langle \alpha j_{12}LJ|\Delta V(R)|\alpha j_{12}LJ\rangle + \frac{L(L+1)}{2\mu R^2} + \varepsilon_{v_1j_1} + \varepsilon_{v_2j_2} \tag{5}
$$

where ΔV is the interaction potential while $\varepsilon_{v_1j_1}$ and $\varepsilon_{v_2j_2}$ are respectively the rovibrational energy of the H_2 and HF monomers when separated. As illustrated in Figure 2, Peak 3 at 5.08 K dominated by the (L, J) = (6, 8) partial wave and Peak 4 at 7.71 K dominated by the (L, J) = (6, 7) partial wave can be readily assigned as shape resonances corresponding to the 1D quasi-bound states at 5.21 and 6.36 K, respectively.

https://doi.org/10.1021/acs.jpclett.4c03703
J. Phys. Chem. Lett. 2025, 16, 1796−1801

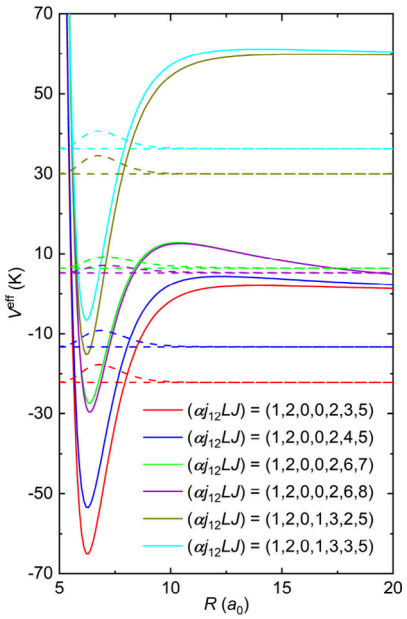

Figure 2. One-dimensional effective potential energy curves and the probability density $\rho(R)$ for bound or quasi-bound states supported. The initial states are indicated for different curves. The inclusion of the α = (1,2,0,1) states is aimed at explaining why Feshbach resonance supported by a single closed channel was ruled out in assigning Peaks 1 and 2.

However, the 1D model for the (L, J) = (3, 5) or (4, 5) case does not show any quasi-bound state. Moreover, the energies of two lowest-lying bound states with different parity supported by closed channels, specifically $(\alpha j_{12} LJ)$ = (1,2,0,1,3,2,5) and (1,2,0,1,3,3,5), are ∼30 K higher than the resonance energies, which ruled out Feshbach resonances. Therefore, this 1D model is insufficient to assign the two resonance peaks below 3 K.

To gain more definitive information on these low-lying resonances, we determine the corresponding wavefunctions by diagonalizing the full-dimensional Hamiltonian using a stabilization method ($\hbar$ = 1):[27]

$$H = -\frac{1}{2\mu}\frac{\partial^2}{\partial R^2} + \frac{\mathbf{L}^2}{2\mu R^2} + h_1 + h_2 + \Delta V \tag{6}$$

where h_1 and h_2 are respectively the asymptotic Hamiltonian for H_2 and HF monomers. To understand stereodynamics, the eigenfunctions are expressed in the SF frame for fixed J, ε and M

$$|\tilde{\Phi}^{JM\varepsilon}\rangle = \sum_{p\alpha j_{12} L} G^{J\varepsilon}_{p\alpha j_{12} L} |X_p\rangle |v_1 j_1\rangle |v_2 j_2\rangle |j_1 j_2 j_{12} LJM\rangle \tag{7}$$

where the expansion basis is defined in Section S−IV of SI.

To assign the resonance states, we examine the following weight for the channel $\alpha j_{12} LJ$:

$$P^{J\varepsilon}_{\alpha j_{12} L} \equiv \sum_p |G^{J\varepsilon}_{p\alpha j_{12} L}|^2 \tag{8}$$

For a shape resonance related to a specific open entrance or exit channel $(\alpha j_{12} LJ)$, the corresponding $P^{J\varepsilon}_{\alpha j_{12} L}$ would be large. For a Feshbach resonance, on the other hand, the largest $P^{J\varepsilon}_{\alpha j_{12} L}$ value would be for a closed channel corresponding to an internally excited entrance (or exit) state.

Four quasi-bound states were found at 0.56 (State 1, J = 5, ε = −1), 2.53 (State 2, J = 5, ε = +1), 5.06 (State 3, J = 8, ε = +1), and 7.62 K (State 4, J = 7, ε = +1), which correspond the four resonance peaks, respectively, in agreement with the results of TICC calculations shown in Figure 1(a). All are dominated by the entrance CMS α = (1,2,0,0), as shown in Table 1, which can be safely assigned as shape resonances.

Table 1. Information of the Four Resonance States Labelled by a Single J and ε[a]

State	Energy/K	$L_{scatt.}$	$L_{res.}$	$P^{J\varepsilon}_{\alpha j_{12} L_{res.}}$
1	0.56	3	5	0.52
2	2.53	4	4	0.71
3	5.06	6	6	0.82
4	7.62	6	6	0.79

[a]All are dominated by channels where α = (1, 2, 0, 0) and j_{12} = 2. $L_{scatt.}$ is the partial wave responsible for the resonance. The largest $P^{J\varepsilon}_{\alpha j_{12} L_{res.}}$ weights along with corresponding $L_{res.}$ are listed

Moreover, it is noteworthy that Peak 1 is attributed to the L = 3 partial wave, while State 1 is dominated by L = 5 channel, which highlights the nonnegligible role of coupling between different scattering channels in the strongly interacting region, especially those featured by same CMSs but different L values. We also found that the L = 5 incoming partial wave led to a scattering resonance and dominated by the (L, J) = (5, 5) component at 0.52 K as seen in Figure S4. This behavior of the (L, J) = (5, 5) incoming partial wave reinforces the importance of the L = 5 channel for State 1. However, the contribution of the (L, J) = (5, 5) incoming partial wave is too small to impact on the total ICS. This can be attributed to the preference for the smaller angular momentum (L = 3) instead of the larger (L = 5) in the entrance channel in cold collisions.

In SF coordinates illustrated in Figure S1, two-dimensional cuts of quasi-bound wavefunctions $\tilde{\Phi}^{J0\varepsilon}$ as a function of R and ϕ_1 are shown in Figure 3. In these cuts, all the other seven coordinates are fixed with the azimuthal angles ϕ and ϕ_2 at right angles. It is clear that States 1 and 3 are symmetric about ϕ_1 = 90°, whereas States 2 and 4 are antisymmetric featuring a node at 90°. The different symmetries hold clues to their different behaviors in stereodynamics.

To further understand the stereodynamics controlled by the shape resonances, we have developed a new model in the SF frame. A resonance state $|\Phi^{JM\varepsilon}(E)\rangle$ labeled by J, M and ε can be represented in terms of scattering eigenstates $|\Psi^{+}_{\alpha m_1 m_2 L m_L}(E)\rangle$:

$$|\Phi^{JM\varepsilon}(E)\rangle = \sum_{\alpha m_1 m_2 L m_L} A^{JM\varepsilon}_{\alpha m_1 m_2 L m_L}(E) |\Psi^{+}_{\alpha m_1 m_2 L m_L}(E)\rangle \delta_{m_1+m_2+m_L,M} \tag{9}$$

where m_L is the z-component of $\mathbf{L}$ in the SF frame. Here, $|A^{JM\varepsilon}_{\alpha m_1 m_2 L m_L}(E)|^2$ can be interpreted as the probability of $|\Psi^{+}_{\alpha m_1 m_2 L m_L}(E)\rangle$ in the resonance state $|\Phi^{JM\varepsilon}(E)\rangle$. Numerically, the resonance wavefunction $\tilde{\Phi}^{JM\varepsilon}(E)$ determined by the stabilization method is expected to be a good approximation of $\Phi^{JM\varepsilon}(E)$ in the strongly interacting region.[27] A scaled quantity $\tilde{A}^{JM\varepsilon}_{\alpha m_1 m_2 L m_L}(E) \propto A^{JM\varepsilon}_{\alpha m_1 m_2 L m_L}(E)$ can be generated by an integral related to centrifugal and interaction potentials as shown in Section S−V of SI. This quantity is dominated by the behavior of $\tilde{\Phi}^{JM\varepsilon}(E)$ at small R.

https://doi.org/10.1021/acs.jpclett.4c03703
J. Phys. Chem. Lett. 2025, 16, 1796−1801

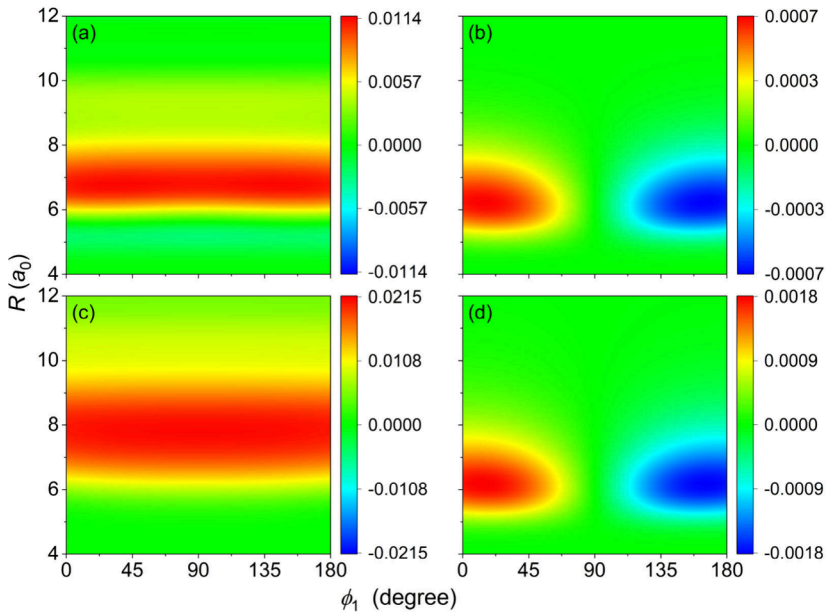

Figure 3. Cuts of wavefunctions $\tilde{\Phi}^{J0\varepsilon}$ in a.u. for State 1 (a), 2 (b), 3 (c), and 4 (d) with $r_1 = 1.405a_0$, $r_2 = 1.735a_0$, $\theta = 0$, $\theta_1 = 80°$, $\theta_2 = 160°$, and $\phi = \phi_2 = 90°$.

Generally, more than one m_1 and m_2 contributes to the incoming wave in a SARP experiment. The overall importance of the resonance can thus be written as

$$\tilde{W}_{\alpha L;\text{aligned},\beta} = \frac{1}{2j_2 + 1} \sum_{M,m_1,m_2} |d^{j_1}_{0,m_1}(\beta)|^2 |\tilde{A}^{JM\varepsilon}_{\alpha m_1 m_2 L0}(E)|^2 \delta_{m_1+m_2,M} \tag{10}$$

while in nonpolarized case, we have

$$\tilde{W}_{\alpha L;\text{unaligned}} = \frac{1}{(2j_1 + 1)(2j_2 + 1)} \sum_{M,m_1,m_2} |\tilde{A}^{JM\varepsilon}_{\alpha m_1 m_2 L0}(E)|^2 \delta_{m_1+m_2,M} \tag{11}$$

Derivations of the above formulas are provided in Section S−V of SI.

In Table 2, the calculated values of $\tilde{W}$ are listed, which provide an explanation of the stereodynamics shown in Figure 1(b). Here, $\tilde{W}_{\alpha L;\text{aligned},0}$ and $\tilde{W}_{\alpha L;\text{aligned},90°}$ refer to H-SARP and V-SARP, respectively. The vanishing $\tilde{W}_{\alpha L;\text{aligned},0}$ for States 2 ($L = 4, J = 5$) and 4 ($L = 6, J = 7$) can be attributed to the fact that only $|\Psi^{+}_{\alpha 00L0}(E)\rangle$ contributes in both cases and $\tilde{W}_{\alpha L;\text{aligned},0} = |\tilde{A}^{J0\varepsilon}_{\alpha 00L0}|^2 \propto |\langle j_{12} 0L0|J0\rangle|^2 = 0$ ($j_{12} = 2$). This signifies that head-on collision is incompatible with these resonances, in complete agreement with the results of scattering calculations. This propensity can be traced to symmetry. It can be easily shown (see Section S−VI of SI) that both $|\tilde{\Phi}^{J0\varepsilon}(E)\rangle$ and $|\Phi^{J0\varepsilon}(E)\rangle$ are antisymmetric with respect to the reflection in the $y^{\text{SF}}z^{\text{SF}}$ plane of SF frame σ^{SF}_{yz}, while $|\Psi^{+}_{\alpha 00L0}(E)\rangle$ is symmetric. Hence, the overlap between $|\Psi^{+}_{\alpha 00L0}(E)\rangle$ and $|\Phi^{J0\varepsilon}(E)\rangle$ is rigorously zero and corresponding resonance transition is forbidden. Note that $\phi = \phi_1 = \phi_2 = 90°$ when both H_2 and HF are in the $y^{\text{SF}}z^{\text{SF}}$ plane, so wavefunction cuts with $\phi = \phi_2 = 90°$ in Figure 3 reflect the reflection symmetry with respect to $y^{\text{SF}}z^{\text{SF}}$ plane.

Table 2. Calculated $\tilde{W}_{\alpha L;\text{unaligned}}$, $\tilde{W}_{\alpha L;\text{aligned},0}$ (H-SARP), and $\tilde{W}_{\alpha L;\text{aligned},90°}$ (V-SARP) Values in 10^{-10} a.u. for the Four Resonances

State	Energy/K	$\tilde{W}_{\alpha L;\text{unaligned}}$	$\tilde{W}_{\alpha L;\text{aligned},0}$	$\tilde{W}_{\alpha L;\text{aligned},90°}$
1	0.56	1.69	2.56	1.31
2	2.53	53.24	0	63.53
3	5.06	29.04	47.83	21.57
4	7.62	89.98	0	101.23

On the contrary, no significant difference was found between $\tilde{W}_{\alpha L;\text{aligned},0}$ and $\tilde{W}_{\alpha L;\text{unaligned}}$ for States 1 and 3, which indicates the corresponding resonances will survive when H_2 is aligned by H-SARP. Besides, $\tilde{W}_{\alpha L;\text{aligned},90°}$ for all four resonances are close to $\tilde{W}_{\alpha L;\text{unaligned}}$, suggesting a small impact of V-SARP, as shown in Figure 1(b).

This model can be easily extended to other polyatomic systems. Instead of its asymptotic behavior, properties of a shape resonance wavefunction in the strongly interacting region are considered. A remarkable result of this model is the natural emergence of a new propensity rule on initial alignment of collisional partners.

In conclusion, we have investigated quantum dynamics in cold collisions, using the *para*-H_2 ($v_1 = 1, j_1 = 2$) + HF ($v_2 = 0, j_2 = 0$) → *para*-H_2 ($v'_1 = 1, j_1' = 0$) + HF ($v'_2 = 0, j_2'$) system as an example. Multiple resonance peaks were identified at collision energies near 1 K and found to response to the initial alignment of the H_2 molecule. Interestingly, these shape resonances cannot be all assigned by the commonly used 1D model, due apparently to strong coupling between different scattering channels. Using a stabilization method, the wavefunctions of these quasi-bound states are obtained in full dimensionality and they manifest multidimensional characteristics due apparently to the strong anisotropy of the PES. We further demonstrate that stereodynamics can be rationalized by the dependence of the resonance wavefunctions on the initial orientation/alignment of the collider, without resorting to state-to-state S matrix elements. This approach can be readily extended to polyatomic collisional partners, where strong potential anisotropy is expected to render scattering resonances strongly coupled in a multidimensional space.

https://doi.org/10.1021/acs.jpclett.4c03703
J. Phys. Chem. Lett. 2025, 16, 1796−1801

■ ASSOCIATED CONTENT

Supporting Information

The Supporting Information is available free of charge at https://pubs.acs.org/doi/10.1021/acs.jpclett.4c03703.

Details of the coordinate systems, long-range potential energy surface, integral cross sections for $j_2' = 0, 1, 2$ and 3, basis functions in the space-fixed frame, new model for stereodynamics and proof of reflection symmetry of wavefunctions (PDF)

Transparent Peer Review report available (PDF)

■ AUTHOR INFORMATION

Corresponding Authors

Yilang Liu − *Institute of Theoretical and Computational Chemistry, Key Laboratory of Mesoscopic Chemistry, School of Chemistry and Chemical Engineering, Nanjing University, Nanjing, Jiangsu 210023, China; Department of Chemistry and Chemical Biology, Center for Computational Chemistry, University of New Mexico, Albuquerque, New Mexico 87131, United States*; Email: 652022240010@smail.nju.edu.cn

Daiqian Xie − *Institute of Theoretical and Computational Chemistry, Key Laboratory of Mesoscopic Chemistry, School of Chemistry and Chemical Engineering, Nanjing University, Nanjing, Jiangsu 210023, China; Hefei National Laboratory, Hefei, Anhui 230088, China;* orcid.org/0000-0001-7185-7085; Email: dqxie@nju.edu.cn

Authors

Dongzheng Yang − *Department of Chemistry and Chemical Biology, Center for Computational Chemistry, University of New Mexico, Albuquerque, New Mexico 87131, United States; Hefei National Research Center for Physical Sciences at the Microscale, University of Science and Technology of China, Hefei, Anhui 230026, China;* orcid.org/0000-0002-8567-1051

Hua Guo − *Department of Chemistry and Chemical Biology, Center for Computational Chemistry, University of New Mexico, Albuquerque, New Mexico 87131, United States;* orcid.org/0000-0001-9901-053X

Complete contact information is available at: https://pubs.acs.org/10.1021/acs.jpclett.4c03703

Notes

The authors declare no competing financial interest.

■ ACKNOWLEDGMENTS

This work was supported by the Innovation Program for Quantum Science and Technology (2021ZD0303305 to D. X.) and National Natural Science Foundation of China (Grant Nos. 22233003 and 22241302 to D.X.). The UNM team acknowledges support of US DOE (DE-SC0015997 to H. G.).

■ REFERENCES

(1) Levine, R. D. *Quantum Mechanics of Molecular Rate Processes*; Clarendon, 1969.

(2) Orr-Ewing, A. J. Dynamical sterochemistry of bimolecular reactions. *J. Chem. Soc. Faraday* **1996**, *92*, 881.

(3) Alexander, A. J.; Brouard, M.; Kalogerakis, K. S.; Simons, J. P. Chemistry with a sense of direction—the stereodynamics of bimolecular reactions. *Chem. Soc. Rev.* **1998**, *27*, 405−415.

(4) van de Meerakker, S. Y. T.; Bethlem, H. L.; Vanhaecke, N.; Meijer, G. Manipulation and control of molecular beams. *Chem. Rev.* **2012**, *112*, 4828−4878.

(5) Aoiz, F. J.; Brouard, M.; Gordon, S. D. S.; Nichols, B.; Stolte, S.; Walpole, V. A new perspective: imaging the stereochemistry of molecular collisions. *Phys. Chem. Chem. Phys.* **2015**, *17*, 30210−30228.

(6) Liu, K. Vibrational control of bimolecular reactcions with methane with mode-, bond-, and stereo-selectivity. *Annu. Rev. Phys. Chem.* **2016**, *67*, 91−111.

(7) Heid, C. G.; Walpole, V.; Brouard, M.; Jambrina, P. G.; Aoiz, F. J. Side-impact collisions of Ar with NO. *Nat. Chem.* **2019**, *11*, 662−668.

(8) Mukherjee, N. Quantum-controlled collisions of H_2 molecules. *J. Phys. Chem. A* **2023**, *127*, 418−438.

(9) Jiang, B.; Cheng, C.; Yang, D.; Guo, H.; Xie, D.; Shen, X. Dynamics of collision-induced energy transfer. *Fundam. Res.* **2023** DOI: 10.1016/j.fmre.2023.09.010.

(10) Wang, Y.; Huang, J.; Wang, W.; Du, T.; Xie, Y.; Ma, Y.; Xiao, C.; Zhang, Z.; Zhang, D. H.; Yang, X. Stereodynamical control of the H + HD → H_2 + D reaction through HD reagent alignment. *Science* **2023**, *379*, 191−195.

(11) Krems, R. V. Cold controlled chemistry. *Phys. Chem. Chem. Phys.* **2008**, *10*, 4079−4092.

(12) Balakrishnan, N. Perspective: Ultracold molecules and the dawn of cold controlled chemistry. *J. Chem. Phys.* **2016**, *145*, 150901.

(13) Perreault, W. E.; Mukherjee, N.; Zare, R. N. Quantum control of molecular collisions at 1 K. *Science* **2017**, *358*, 356−359.

(14) Perreault, W. E.; Mukherjee, N.; Zare, R. N. Cold quantum-controlled rotationally inelastic scattering of HD with H_2 and D_2 reveals collisional partner reorientation. *Nat. Chem.* **2018**, *10*, 561−567.

(15) Zhou, H.; Perreault, W. E.; Mukherjee, N.; Zare, R. N. Shape resonance determined from angular distribution in D_2 (v = 2, j = 2) + He → D_2 (v = 2, j = 0) + He cold scattering. *J. Chem. Phys.* **2021**, *154*, 104309.

(16) Zhou, H.; Perreault, W. E.; Mukherjee, N.; Zare, R. N. Anisotropic dynamics of resonant scattering between a pair of cold aligned diatoms. *Nat. Chem.* **2022**, *14*, 658−663.

(17) Croft, J. F. E.; Balakrishnan, N.; Huang, M.; Guo, H. Unraveling the stereodynamics of cold controlled HD-H_2 collisions. *Phys. Rev. Lett.* **2018**, *121*, 113401.

(18) Jambrina, P. G.; Croft, J. F. E.; Guo, H.; Brouard, M.; Balakrishnan, N.; Aoiz, F. J. Stereodynamical control of a quantum scattering resonance in cold molecular collisions. *Phys. Rev. Lett.* **2019**, *123*, 043401.

(19) Jambrina, P. G.; Croft, J. F. E.; Zuo, J.; Guo, H.; Balakrishnan, N.; Aoiz, F. J. Stereodynamical control of cold collisions between two aligned D_2 molecules. *Phys. Rev. Lett.* **2023**, *130*, 033002.

(20) Balakrishnan, N.; Jambrina, P. G.; Croft, J. F. E.; Guo, H.; Aoiz, F. J. Quantum stereodynamics of cold molecular collisions. *Chem. Commun.* **2024**, *60*, 1239−1256.

(21) Morita, M.; Yao, Q.; Xie, C.; Guo, H.; Balakrishnan, N. Stereodynamic control of overlapping resonances with aligned cold molecular collisions. *Phys. Rev. Res.* **2020**, *2*, No. 032018(R).

(22) Guillon, G.; Stoecklin, T.; Voronin, A.; Halvick, P. Rotational relaxation of HF by collision with ortho- and para-H_2 molecules. *J. Chem. Phys.* **2008**, *129*, 104308.

(23) Yang, D.; Huang, J.; Zuo, J.; Hu, X.; Xie, D. A full-dimensional potential energy surface and quantum dynamics of inelastic collision process for H_2−HF. *J. Chem. Phys.* **2018**, *148*, 184301.

(24) Huang, J.; Zhou, Y.; Xie, D. Predicted infrared spectra in the HF stretching band of the H_2−HF complex. *J. Chem. Phys.* **2018**, *149*, 094307.

(25) Yang, D.; Hu, X.; Zhang, D. H.; Xie, D. An improved coupled-states approximation including the nearest neighbor Coriolis couplings for diatom-diatom inelastic collision. *J. Chem. Phys.* **2018**, *148*, 084101.

(26) Schaefer, J.; Meyer, W. Theoretical studies of H_2-H_2 collisions. I. Elastic scattering of ground state para- and ortho-H_2 in the rigid rotor approximation. *J. Chem. Phys.* **1979**, *70*, 344−360.

(27) Hazi, A. U.; Taylor, H. S. Stabilization method of calculating resonance energies: Model problem. *Phys. Rev. A* **1970**, *1*, 1109−1120.

https://doi.org/10.1021/acs.jpclett.4c03703
J. Phys. Chem. Lett. 2025, 16, 1796−1801